Unified Statistical Framework for Rotor Fault Diagnosis on a Hexacopter via Functionally Pooled Stochastic Models

Airin Dutta PhD Student
Robert Niemiec Lecturer
Fotis Kopsaftopoulos Assistant Professor
Farhan Gandhi Redfern Professor Director

Center for Mobility with Vertical Lift (MOVE)
Rensselaer Polytechnic Institute, Troy, NY

ABSTRACT

In this work, a statistical time series method that is capable of effective multicopter rotor fault detection, identification, and quantification within a unified stochastic framework is introduced. The proposed framework is based on the functional model based method for fault magnitude estimation tackled within the context of statistical time series approaches. Estimator uncertainties are taken into account, and confidence intervals are provided for the fault magnitude of multicopter rotors. The framework employs functionally pooled (FP) models which are characterized by parameters that depend on the fault magnitude, as well as on proper statistical estimation and decision-making schemes. The validation and assessment is assessed via a proof-of-concept application to a hexacopter flying forward with a constant velocity under turbulence. The fault scenarios considered consist of the front and side rotor degradation ranging from healthy to complete failure with 20% fault increments. The method is shown to achieve fast fault detection, accurate identification, and precise magnitude estimation based on even a single measured signal obtained from aircraft sensors during flight. Furthermore, fault quantification is addressed via the use of both local (boom acceleration) and global (IMU) sensors, with the signals collected from the boom supporting the identified faulty rotor proven to achieve better performance than the global signals, yet with a shorter signal length.

NOTATION

α	:	Type I risk level
ρ	:	Normalized Autocorrelation
τ	:	Lag
θ	:	Model parameter vector
χ^2	:	Chi-square distribution
σ^2	:	Residual variance
$\mathcal{N}$	:	Gaussian distribution
$E\{\cdot\}$	:	Expected value
CRLB	:	Cramér-Rao Lower Bound
IMU	:	Inertial Measurement Unit
PSD	:	Power Spectral Density
BIC	:	Bayesian Information Criterion
RSS	:	Residual Sum of Squares
ACF	:	Auto-Covariance Function
iid	:	identically independently distributed
OLS	:	Original Least Squares
SSS	:	Signal Sum of Squares
AR	:	Scalar AutoRegressive model
FP	:	Functionally Pooled
WLS	:	Weighted Least Squares

Presented at the Vertical Flight Society's 77th Annual Forum & Technology Display, Virtual, May 10–14, 2021 .

INTRODUCTION

Urban air mobility (UAM), enabled by autonomous electric VTOL (eVTOL) aircraft is set to revolutionize urban transport. A NASA sponsored study concluded UAM is a viable option and assessed its available market value at $500B (Ref. 1). But, the operational success of on-demand aviation service for mass transportation requires absolute safety and reliability. The preliminary safety target of UAM utilizing the airspace over dense urban environments has been established to be twice as safe as driving by Uber Elevate (Ref. 2), with the expected improvement toward airline aviation levels of safety through innovation with full autonomy and large amounts of data from real-world operations after the first generation VTOL aircraft are in production. Therefore, the current interest is towards real-time system-level awareness and safety assurance in UAM aircraft utilizing in-flight data streams. The goal of this line of work is the development of a data-driven and probabilistic rotor fault diagnosis framework in multicopters which will provide online information about rotor faults, critical for control reallocation or vehicle reconfiguration to complete the flight safely.

Multicopters have been identified as a potential platform for future UAM aircraft development due to their rotor redundancy, design flexibility, ability to integrate dis-

tributed electric propulsion, and their superior fault robustness and compensation capabilities. These are complex systems that exhibit strong non-linear dynamic coupling between rotors, structural components, fuselage, and control inputs, as well as time-varying and cyclostationary behavior and pose significant system modeling and identification challenges when compared to fixed-wing aircraft. These issues, as well as potential solutions, have been explored in the recent literature. Fault-tolerant control for multi-rotors (Refs. 3, 4), as well as various fault diagnosis methods for rotorcraft have been proposed (Refs. 5–10). However, the methods discussed in the above papers suffer from the requirement of analytical modeling, knowledge of system properties like mass, rotor inertia, etc., and the use of arbitrary deterministic thresholds for tackling rotor FDI. These limitations are collectively addressed in this work via the use of stochastic time series representations of the multicopter dynamics based on flight signals without requiring knowledge of the system properties. Also, the rotor fault diagnosis approaches will be developed within a statistical framework that inherently accounts for operating and environmental uncertainty through properly defined statistical thresholds under predetermined confidence levels. Towards this end, statistical time series methods have been explored thoroughly in this work.

Statistical time series methods have been used to detect various fault types in aircraft systems due to their simplicity, efficient handling of uncertainties, no requirement of physics-based models, and applicability to different operating conditions (Refs. 11–14). Reliable fault detection, identification, and isolation have been achieved in fixed-wing aircraft under unknown external disturbances, various maneuvering settings, and fault scenarios by modeling relationships among aircraft attitude data and pilot inputs via stochastic Time-dependent Functionally Pooled Non-linear AutoRegressive with Exogenous excitation (TFP-NARX) (Ref. 15) and Pooled Non-Linear AutoRegressive Moving Average with eXogenous excitation (P-NARMAX) (Ref. 16) representations. Kopsaftopoulos and Fassois achieved statistical damage localization and estimation by formulation of Vector-dependent Functionally Pooled ARX (VFP-ARX) models identified with vibration-based data pooled from different damage sizes and locations and uncertainty. This constitutes a "global" model of the structure, whose parameters are functionally dependent on the operating variables (Refs. 17, 18). This identification framework incorporates parsimonious VFP models that can fully account for cross correlations among the operating conditions, perform functional pooling for the simultaneous treatment of all data records, and achieve statistically optimal parameter estimation based on Least Squares (LS) and Maximum Likelihood (ML) schemes. Previously, Dutta *et al.* achieved fast and accurate online rotor fault detection and identification *via*a novel application of statistical time-series methods to multicopters flying forward under different turbulence levels and uncertainty as well as varying forward velocity and gross weight in Refs. 19, 20. However, literature pertaining to actuator fault quantification is scarce. This information obtained online can facilitate switching over to a more optimal control scheme and planning alternative trajectories with limited control authority depending on the fault severity. Therefore, to fill this research gap an innovative time-series assisted neural network with improved explainability was proposed. Its excellent FDI performance with regard to determining three discrete fault levels (mild, caution, and urgent) in addition to simultaneous detection and classification was demonstrated in Refs.21, 22.

The objective of this paper is the introduction, assessment, and proof-of-concept study of a unified statistical framework for rotor fault detection, identification, and continuous quantification in multicopters flying forward under external disturbances and uncertainty. Functionally pooled (FP) model-based methods used for vibration-based structural health monitoring, provide an integrated framework for damage detection, localization, and quantification. This family of methods allows for consideration of the damage magnitude in a continuous fashion (Ref. 23). The current study investigates a novel application of the above methods in the context of probabilistic fault diagnosis on a hexacopter using sensor data (time-series signals). The cornerstone of the proposed framework lies in the stochastic time-series representation of the aircraft dynamics via FP stochastic models that can account different types and magnitude of rotor degradation, turbulence, and uncertainty. These models can subsequently enable online fault detection, identification, and quantification via statistical decision-making schemes under predetermined confidence levels (type I error probabilities, i.e., false alarms).

HEXACOPTER MODEL AND DATA GENERATION

Physics-Based Modeling of Multicopter System

A flight simulation model has been developed for a regular hexacopter (Fig. 1) using summation of forces and moments to calculate aircraft accelerations. This model is used as the source of simulated data under varying operating and environmental conditions, as well as different fault types. Rotor loads are calculated using Blade Element Theory coupled with a 3×4 Peters-He finite state dynamic wake model (Ref. 24). This model allows for the simulation of abrupt rotor failure by ignoring the failed rotor inflow states and setting the output rotor forces and moments to zero.

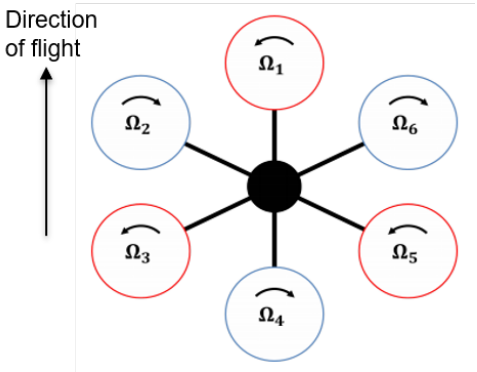

Figure 1: Schematic representation of a regular hexacopter

A feedback controller is implemented on the nonlinear model to stabilize the aircraft altitude and attitudes, as well as track desired trajectories written in terms of the aircraft velocities. This controller is designed at multiple trim points, with gain scheduling between these points to improve performance throughout the flight envelope. The control architecture is detailed in Ref. 3. This control design has been demonstrated to perform well even in the event of rotor 1, 2 or 6 failure, with no adaptation in the control laws themselves.

The 12 rigid body states are defined in Eq. 1.

$$\mathbf{x} = \begin{Bmatrix} X & Y & Z & \phi & \theta & \psi & u & v & w & p & q & r \end{Bmatrix}^T \tag{1}$$

The input vector is comprised of the first four independent multirotor controls for collective, roll, pitch and yaw and is defined in Eq. 2:

$$\mathbf{u} = \begin{Bmatrix} \Omega_0 & \Omega_R & \Omega_P & \Omega_Y \end{Bmatrix}^T \tag{2}$$

The booms of the hexacopter are modeled as one-dimensional, Euler-Bernoulli beams, with an added tip mass and loading, and are coupled to the rigid body motion of the vehicle. The positive bending deflections in the in-plane and out-of plane of the hub are illustrated in Fig. 2. Torsion is neglected. The beam equations are discretized in space using the Ritz method with 2 modes in direction, as given in Eq. 3), with polynomial shape functions, ϕ that satisfy the geometric boundary conditions given by Eq. 4. To facilitate the inversion of the mass matrix that arises from this discretization, these polynomials are chosen to be orthogonal. The modes are obtained via eigen-analysis of the beam in a vacuum.

$$\begin{aligned} v &= \sum_{i=1}^{2} \eta_{v_i}(t)\phi_{v_i}(l) \\ w &= \sum_{i=1}^{2} \eta_{w_i}(t)\phi_{w_i}(l) \end{aligned} \tag{3}$$

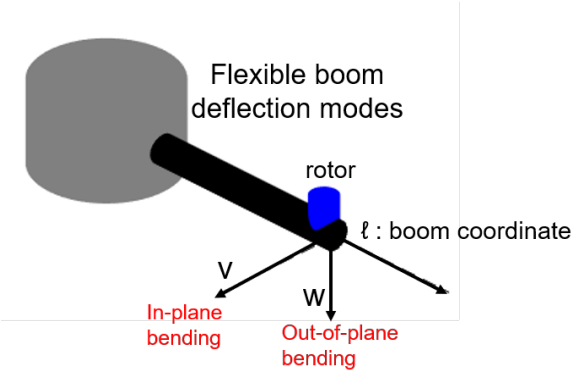

Figure 2: Flexible boom deformation

where, η represents the modal deformations. l is the non-dimensional boom coordinate, representing the distance of a point on the boom from its root normalized by the boom length. It ranges from 0 to 1, denoting the boom root and boom tip, respectively. The geometric boundary conditions are given by:

$$\begin{aligned} w(0) = w'(0) = 0 \\ v(0) = v'(0) = 0 \end{aligned} \tag{4}$$

The 8 flexible states for each boom are defined as follows:

$$\mathbf{x} = \begin{Bmatrix} \eta_{w_1} & \eta_{w_2} & \eta_{v_1} & \eta_{v_2} & \dot{\eta}_{w_1} & \dot{\eta}_{w_2} & \dot{\eta}_{v_1} & \dot{\eta}_{v_2} \end{Bmatrix}^T \tag{5}$$

In the above equations, ' ′ ' and ' ˙ ' imply $\frac{d}{dl}$ and $\frac{d}{dt}$, respectively.

Data Generation

A continuous Dryden wind turbulence model (Ref. 25) has been implemented in the flight simulation model. The Dryden model is dependent on altitude, length scale, and turbulence intensity and outputs the linear and angular velocity components of continuous turbulence as spatially varying stochastic signals. The proper combination of these parameters determines the fit of the signals to observed turbulence. In this system, altitude is taken as 5 m (16.4 ft) and the length scale as the hub-to-hub distance of the hexacopter, which is 0.6096 m (2 ft). The data sets are generated through a series of simulations for different fault types and magnitude under severe of turbulence for the aircraft flying at 5 m/s and having a gross weight of 2 kg. Note that the rotor failures addressed in this paper are: front rotor (rotor 1) and the right-side rotor (rotor 2)(See Fig. 1). Rotor degradation has been replicated by reducing the commanded speed of that particular rotor by a multiplier ranging from 0 to 1.

The rotor fault diagnosis is based on output signals recorded from simulations at a sampling frequency, $F_s =$

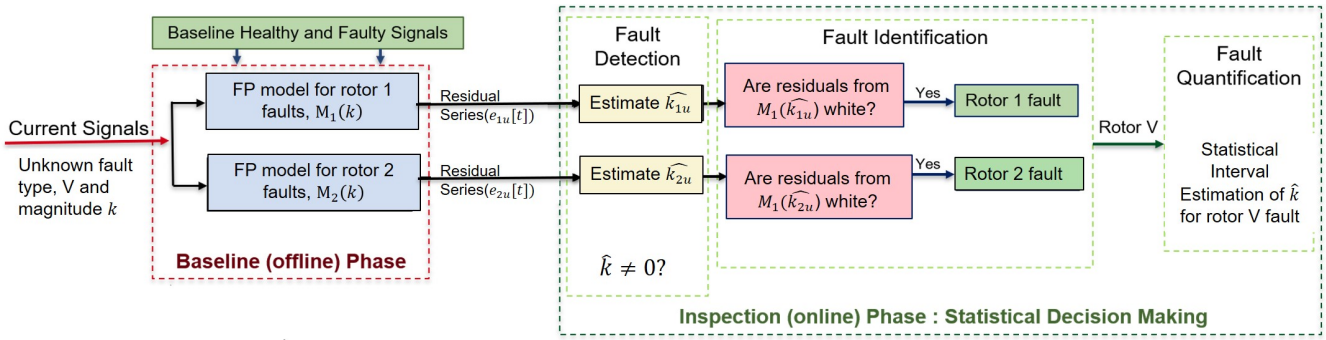

Figure 3: General Workframe of unified statistical time series framework for rotor fault detection, identification, and quantification.

Table 1: Data

Rotor Type	Degradation levels (%)
Rotor 1	$0, 10, 20, \ldots, 100$
Rotor 2	$0, 10, 20, \ldots, 100$
Signal length: 60 s, Sampling frequency F_s: 10 kHz	
For rotor degradation signals, failure happens at 10 s	
Degradation % 0: healthy, 100: complete failure	
Forward velocity: 5 m/s, Gross weight: 2 kg	
Turbulence level: Severe	

10 kHz, to capture the flexible boom natural frequencies. In this study, the output signals considered are of two types: local and global sensor readings. The global sensor readings are the signals obtained from the aircraft Inertial Measurement Unit (IMU) located at the hub, which measures the aircraft accelerations and the attitude rates. The local sensor readings are obtained from the strain gauges or accelerometers placed at the individual rotor booms. The sensor signals are calculated using the aircraft states obtained from the flight simulation (See Appendix A). Data at 0, 10, 20,...,100 % degradation of rotor 1 and 2 at forward velocity of 5 m/s and 2 kg gross weight were generated. Degradation of 0 % and 100 % implies healthy flight and complete rotor failure, respectively. Data at 0, 20, 40, 60, 80, and 100 were used as the training data for model identification and the subsequent development of the residual-based methods. The rest of the data sets were reserved as test data for validating the models and methods under "unmodelled" (not used in baseline modeling) operating conditions, like fault magnitude 10, 30, 50, 70, and 90 % of rotor 1 and 2.

FAULT DETECTION, IDENTIFICATION AND QUANTIFICATION FRAMEWORK

Let Z_o be signals that designate the aircraft under consideration in its healthy state, and Z_1, Z_2 and Z_6 the aircraft under fault of Rotor 1, and 2. Z_u designates the unknown (to be determined) state of the aircraft. Statistical learning methods explored in this study are based on discretized aircraft states signals $y[t]$[1] only (for $t = 1, 2, \ldots, N$). N denotes the number of samples and the conversion from discrete normalized time to analog time is based on $(t-1)T_s$, with T_s being the sampling period. The signals are represented by Z and subscript $(o, 1, 2, u)$ is used to denote the corresponding state of the aircraft that produced the signals. The signals generated from the simulation are analyzed by non-parametric followed by parametric statistical methods and proper models are fitted and validated.

The unified statistical framework for multicopter rotor fault detection, identification, and subsequent quantification is depicted in Fig. 3. Here, the idea is to construct one FP model for each of the rotors/ fault types ($V = 1, 2$) in the baseline phase which will include rotor degradation as the functional variable, ranging from healthy aircraft to complete rotor failure. Therefore, operating state vector, k will contain the extent of rotor degradation (k_i). Such models are trained with signals Z_1, Z_2 and denoted by $M_1(k), M_2(k)$, respectively. The aim is to estimate the rotor degradation from the current signals in the online phase and enable rotor fault quantification post rotor FDI as illustrated in Fig. 3. The rotor fault type models are re-parameterized with all possible values of rotor degradation and the current signals are filtered through them. The value of fault magnitude that results in minimum error is chosen as the estimated value of rotor degradation, $\hat{k}$. Statistical hypothesis tests are constructed to ascertain whether $\hat{k} = 0$ for all rotor FP models, ensuring that the aircraft is healthy. A fault is detected if any $\hat{k} \neq 0$, and the models are re-parameterized with their corresponding estimate of rotor degradation. Fault identification is based on the fact that the correct rotor model will yield white (serially uncorrelated) residuals for its corresponding es-

[1] A functional argument in parentheses designates function of a real variable; for instance $x(t)$ is a function of analog time $t \in \mathbb{R}$. A functional argument in brackets designates function of an integer variable; for instance $x[t]$ is a function of normalized discrete time $(t = 1, 2, \ldots)$.

timate of $\hat{k}$. Once the fault is identified, that rotor model is used for interval estimation of the rotor fault magnitude. The details of model identification, residual-based inverse optimization techniques to estimate the unknown rotor degradation, and its interval estimate under predetermined confidence levels (type I and II error probabilities, *i.e.* false alarm and missed faults) are discussed in the following sections.

Baseline modeling of the aircraft

Statistical time-series methods employ stochastic models, identified on the basis of available random signal(s) obtained from a system under operational and environmental variability, that describe their time evolution and capture the corresponding system dynamics (input-output relationship from data). Besides no requirement of any physical knowledge of the system, these models are also capable of handling disturbances and uncertainty, which makes them attractive for the current application to fault diagnosis under external disturbances and unexpected faults. In the present scenario, response-only models are explored since the signals were recorded under ambient excitation due to turbulence.

Non-Parametric Identification

As a first step of the analysis, the non-parametric identification of the collected signals is based on the Welch-based power spectral density (PSD) estimate. The discrete Fourier transform of the signal of i-th window is given by:

$$Y_L^{(i)}[j\omega] = \frac{1}{\sqrt{L}} \sum_{t=0}^{L-1} y[t] \cdot w[t] \cdot e^{-j2\pi kt/N} \tag{6}$$

where L denotes the length of the window (w), and ω the frequency. Then, the Welch estimate of the PSD of a discrete-time signal is defined as follows:

$$\hat{S}_{yy}(\omega) = \frac{1}{K} \sum_{i=1}^{K} Y_L^{(i)}[j\omega] \cdot Y_L^{(i)}[-j\omega] \tag{7}$$

where K denotes the number of windows the signal is divided into. The PSD provides a description of the variation in the signal's power versus the frequency. It can provide a preliminary idea on the dynamic content of the signal.

Parametric Identification via Stochastic FP Models

The identification of a Functionally Pooled AutoRegressive (FP-AR) models involves consideration of all rotor degradation levels. The data is generated under the different rotor fault magnitudes covering the required range and represented as follows:

$$\begin{gathered} y_k[t] \quad \text{with} \quad t = 1,2,...,N; \\ k \in \left[k_1, k_2, \ldots, k_{K_1}\right]; \end{gathered} \tag{8}$$

with $y_k[t]$ being the univariate response at an operating condition (rotor state) k_i.

The FP-AR$(na)_{pa}$ model structure is of the following form:

$$\begin{aligned} y_k[t] &= \sum_{i=1}^{na} a_i(k) \cdot y_k[t-i] + e_k[t] \\ e_k[t] &\sim \text{iid}\, \mathcal{N}(0, \sigma_e^2(k)), \qquad k \in \mathbb{R}^1 \\ a_i(k) &= \sum_{j=1}^{pa} a_{i,j} \cdot G_j(k) \\ \mathbb{E}\{e_{k_m}[t] \cdot e_{k_n}[t-\tau]\} &= \gamma_e[k_m, k_n] \cdot \delta[\tau] \end{aligned} \tag{9}$$

where na designates the AutoRegressive (AR) order, $e_k[t]$ the model's residual (one-step-ahead prediction error) sequence, that is a white (serially uncorrelated) zero mean sequence with variance $\sigma_e^2(k)$.This sequence should be serially uncorrelated but potentially cross-correlated with its counterparts corresponding to different simulations (different k's). The symbol $\mathbb{E}\{\cdot\}$ designates statistical expectation, $\delta[\tau]$ the Kronecker delta (equal to unity for $\tau = 0$ and equal to zero for $\tau \neq 0$) , $\mathcal{N}(\cdot,\cdot)$ Gaussian distribution with the indicated mean and variance, and iid stands for identically independently distributed. The AR parameters $a_i(k)$ are modeled as explicit functions of the variable k (which contains the fault magnitude information) by belonging to pa-dimensional functional subspace spanned by the mutually independent basis functions, referred to as the functional basis:

$$\mathscr{F}\langle a_i(k)\rangle \triangleq [G_1(k)\; G_2(k) \ldots G_{pa}(k)] \tag{10}$$

The functional basis consists of univariate orthogonal polynomials of increasing order. In this work, Chebyshev type II polynomials are used as the functional basis and these are described in detail in Appendix B. The constants $a_{i,j}$ designate the AR coefficients of projection onto the functional basis. The identification of such parametric time series models is comprised of two main tasks: parameter estimation and model order selection.

The FP-AR model is parameterized in terms of the parameter vector to be estimated[2] from the measured signals:

$$\widehat{\theta} \triangleq \left[a_{1,1}\;\; a_{1,2}\;\; \ldots\;\; a_{na,pa}\right] \tag{11}$$

[2] A hat designates estimator/estimate of the indicated quantity; for instance, $\widehat{\boldsymbol{\sigma}}$ is an estimator/estimate of $\boldsymbol{\sigma}$.

and can be written in linear regression form as:

$$\begin{aligned} y_k[t] &= \left[\varphi_k^T[t] \otimes \mathbf{G}^T(k)\right] \cdot \theta + e_k[t] \\ y_k[t] &= \phi_k^T[t] \cdot \theta + e_k[t] \end{aligned}$$

where:

$$\begin{aligned} \varphi_k[t] &\triangleq \left[y_k[t-1] \ldots y_k[t-na]\right]^T_{na\times 1} \\ \boldsymbol{G}(k) &\triangleq \left[G_1(k) \ldots G_{pa}(k)\right]^T_{pa\times 1} \\ \theta &\triangleq \left[a_{1,1} \ldots a_{na,pa}\right]^T_{(na\times pa)\times 1} \end{aligned} \tag{12}$$

Pooling together the expressions of the FP-AR model corresponding to all the operating parameters k $(k_1, k_2, \ldots, k_{K_1})$ considered in the simulation yields:

$$\begin{aligned} &\begin{bmatrix} y_{k_1}[t] \\ \vdots \\ y_{k_{K_1}}[t] \end{bmatrix} = \begin{bmatrix} \phi_{k_1}^T[t] \\ \vdots \\ \phi_{k_{K_1}}^T[t] \end{bmatrix} \cdot \boldsymbol{\theta} + \begin{bmatrix} e_{k_1}[t] \\ \vdots \\ e_{k_{K_1}}[t] \end{bmatrix} \\ &\implies \boldsymbol{y}[t] = \boldsymbol{\Phi}[t] \cdot \boldsymbol{\theta} + \boldsymbol{e}[t] \end{aligned} \tag{13}$$

Substituting the data for $t = 1, 2, ..., N$ results in the following expression:

$$\begin{aligned} \boldsymbol{y} &= \boldsymbol{\Phi} \cdot \boldsymbol{\theta} + \boldsymbol{e} \\ &\text{where :} \\ \boldsymbol{y} \triangleq \begin{bmatrix} \boldsymbol{y}[1] \\ \vdots \\ \boldsymbol{y}[N] \end{bmatrix}; \quad \boldsymbol{\Phi} &\triangleq \begin{bmatrix} \boldsymbol{\Phi}[1] \\ \vdots \\ \boldsymbol{\Phi}[N] \end{bmatrix}; \quad \boldsymbol{e} \triangleq \begin{bmatrix} \boldsymbol{e}[1] \\ \vdots \\ \boldsymbol{e}[N] \end{bmatrix} \end{aligned} \tag{14}$$

Notice that despite its resemblance to standard regression, this expression includes a rich structure of interdependencies among the different variables and simulations, which need to be carefully taken into account. Furthermore, the term "functional pooling" signifies the functional dependence of each equation on the operating parameter k (indicating the rotor state). Using the above linear regression framework, the simplest approach for estimating the projection coefficient vector θ is based on minimization of the ordinary least squares (OLS) criterion $J^{OLS} := \frac{1}{N}\sum_{t=1}^{N} \boldsymbol{e}^T[t]\boldsymbol{e}[t]$. A better criterion according to the Gauss–Markov theorem (Ref. 26) is the weighted least squares (WLS) criterion:

$$J^{WLS} := \frac{1}{N}\sum_{t=1}^{N} \boldsymbol{e}^T[t]\boldsymbol{\Gamma}^{-1}_{\boldsymbol{e}[t]}\boldsymbol{e}[t] = \frac{1}{N}\boldsymbol{e}^T[t]\boldsymbol{\Gamma}_{\boldsymbol{e}^{-1}\boldsymbol{e}[t]} \tag{15}$$

which leads to the weighted least squares(WLS) estimator:

$$\widehat{\theta}^{WLS} = \left[\boldsymbol{\Phi}^T\boldsymbol{\Gamma}^{-1}_{\boldsymbol{e}}\boldsymbol{\Phi}\right]^{-1}\left[\boldsymbol{\Phi}^T\boldsymbol{\Gamma}^{-1}_{\boldsymbol{e}}\boldsymbol{y}\right] \tag{16}$$

where $\boldsymbol{\Gamma}_{\boldsymbol{e}} = \mathbb{E}[\boldsymbol{e}\boldsymbol{e}^T]$ ($\boldsymbol{\Gamma}_{\boldsymbol{e}} = \boldsymbol{\Gamma}_{\boldsymbol{e}[t]} \otimes \boldsymbol{I}_N$), where $\boldsymbol{I}_N$ is the $N \times N$ unity matrix) designates the residual covariance matrix, which is practically unavailable. Nevertheless, it may be consistently estimated by applying (in an initial step) ordinary least squares (Ref. 27). Once $\widehat{\theta}^{WLS}$ is obtained, the final residual variance and residual covariance matrix estimates are calculated as:

$$\begin{aligned} \widehat{\sigma}_e^2(k, \widehat{\theta}^{WLS}) &= \frac{1}{N}\sum_{t=1}^{N} e_k^2[t, \widehat{\theta}^{WLS}] \\ \widehat{\boldsymbol{\Gamma}}_{\boldsymbol{e}[t]} &= \frac{1}{N}\boldsymbol{e}[t, \widehat{\theta}^{WLS}]\boldsymbol{e}^T[t, \widehat{\theta}^{WLS}] \end{aligned} \tag{17}$$

The problem of FP-AR model structure selection for a given basis function family consists of model order determination for the AR polynomials and determination of their corresponding functional subspaces. Usually, the AR model order is initially selected via customary model order selection techniques (Bayesian Information Criterion (BIC) and Residual Sum of Squares over Signal Sum of squares (RSS/SSS)) (Ref. 28) from individual datasets corresponding to a single cross-section or operating condition (Ref. 29). A cross-section corresponds to a flight state defined by a particular rotor degradation value, considered in the training dataset. Next, maximum functional subspace dimensionalities are considered, which define the search space of the functional subspace estimation subproblem. The exact subspace dimensionalities are decided by minimization of the BIC with respect to the candidate basis functions as follows:

$$\boldsymbol{p} \triangleq [1, 2, \ldots, K_1]$$

Next, the selection of the final dimensionality may be based on minimization of the BIC (Ref. 30):

$$\begin{aligned} \widehat{\boldsymbol{p}} &= \arg\min_{\boldsymbol{p}} BIC(\boldsymbol{p}) \\ BIC(\boldsymbol{p}) &= \ln \mathbf{L} + dim(\theta) \cdot \ln \frac{K_1}{N} \\ \text{where,} \quad \mathbf{L} &= \sum \sigma_e^2(k_i) \\ &\quad \forall \quad i = 1, ..., K_1 \end{aligned} \tag{18}$$

The Residual sum of Squares over Signal Sum of Squares (RSS/SSS) for all the cross-sections used in model estimation is given by:

$$\begin{aligned} \frac{RSS}{SSS} &= \sum \frac{\sum_{t=1}^{N} e_{k_i}^2[t]}{\sum_{t=1}^{N} y_{k_i}^2[t]} \\ &\quad \forall \quad i = 1, \ldots, K_1 \end{aligned} \tag{19}$$

Fault detection, identification and quantification

For tackling FDI, model residual-based methods use functions of the residual sequences (known as the characteristic quantity, Q) which are obtained by driving the

current signal(s) (Z_u) through the models estimated in the baseline phase for different fault types (M_1, M_2). The key idea is that the residual sequence obtained by a model that truly reflects the current state of aircraft possesses certain distinct properties that are distinguishable from that obtained from the other models. Residual-based methods are chosen over model parameters-based methods because they are computationally faster and therefore better suited for online monitoring since they require no model re-identification in the inspection phase.

Fault Detection Fault detection is based on the re-parameterized FP-AR model of any fault mode (e.g. rotor 1,2,..R), in terms of k (rotor degradation) and $\sigma_e^2(k)$. Thus, the projection coefficients are replaced by the corresponding estimates available from the baseline phase, while k containing the fault magnitude and the residual series variance $\sigma_u^2(k)$ are the current unknown parameters and are estimated from current unknown signal, $y_u[t]$ as follows:

$$\mathbf{M}_V\left(k,\sigma^2(k)\right) \,:\, y_u[t] = \sum_{i=1}^{na} a_i(k)\cdot y_u[t-i] + e_u[t,k] \quad (20)$$

The estimation of the currently unknown parameters k and $\Sigma_e(k)$ based on the current signals, may be achieved via the following optimization:

$$\begin{aligned} \hat{k} &= \underset{k\in\mathbb{R}^m}{\arg\min} \sum_{i=1}^{N} e_u^T[t,k] e_u[t,k] \\ \sigma_u^2(\hat{k}) &= \frac{1}{N}\sum_{t=1}^{N} e_u[t,\hat{k}] e_u^T[t,\hat{k}] \end{aligned} \quad (21)$$

The steepest descent method is used to find the optimum $\hat{k}$.

Assuming that the system is indeed under a rotor fault belonging to rotor type R (or healthy), $\hat{k}$ may be shown to be asymptotically ($N\to\infty$) Gaussian distributed ($\hat{k}\sim\mathcal{N}(k,\sigma_k^2)$) with mean as the true value k and covariance σ_k^2 coinciding with the Cramér-Rao Lower Bound denoted as $\hat{\sigma}_{CRLB}^2$, and expressed as the following:

$$\sigma_u^2(\hat{k}) = \left[\sum_{t=1}^{N}\left[\theta^T\cdot\varphi_u[t]\otimes\frac{\delta\mathbf{G}(k)}{\delta k}|_{\hat{k}}\right]\left[\theta^T\cdot\varphi_u[t]\otimes\frac{\delta\mathbf{G}(k)}{\delta k}|_{\hat{k}}\right]^T\right]^{-1} \quad (22)$$

The derivation of the above expression is provided in Appendix C (Ref. 23).

Since the healthy aircraft corresponds to $k=0$ (zero fault magnitude) for any rotor fault model, fault is detection is based on the following hypothesis testing problem:

$$\begin{array}{lcll} H_0 & : & k=0 & \text{null hypothesis – healthy aircraft} \\ H_1 & : & k\neq 0 & \text{alternate hypothesis – rotor fault} \end{array} \quad (23)$$

Under the null (H_0) hypothesis, the following statistic follows t-distribution with $N-1$ degrees of freedom (which should be adjusted to $N-2$ in case the estimated mean is subtracted from the residual series in the computation of $\hat{\sigma}_k^2$):

$$t = \frac{\hat{k}}{\hat{\sigma}_k} \sim t(N-1) \quad (24)$$

with $\hat{\sigma}_k$ being the positive square root of $\hat{\sigma}_k^2$ (estimated standard deviation of k). This leads to the following test at the α risk level (probability of false alarm, or type I error, that is accepting H_1 although H_0 is true, being equal to α):

$$\begin{array}{rcl} t \geq t_{1-\alpha}(N-1) & \longrightarrow & H_0 \text{ accepted (healthy rotor)} \\ \text{Else} & \longrightarrow & H_1 \text{ accepted (faulty rotor)} \end{array} \quad (25)$$

where t_α designates the t distribution's (with the indicated degrees of freedom) α critical point (defined such that $\mathbb{P}\left[t\leq t_\alpha\right]=\alpha$).

Fault Identification Fault (rotor) identification corresponds to the examination of which one of the available rotor FP-AR models provides, for its estimated $\hat{k}$, a valid representation of the current aircraft dynamics based on residual uncorrelatedness (whiteness) hypothesis testing. The current fault dynamics should correspond to the valid model, which will exhibit an uncorrelated (white) residual sequence for the corresponding $\hat{k}$.

Once a fault is detected, current rotor type determination is based on the successive estimation (using the current data) and validation of the re-parameterized $M_V\left(k,\sigma^2(k)\right)$ FP-AR models for $V=1,2$ corresponding to the different faulty rotors. The procedure stops as soon as a particular model is successfully validated, with the corresponding faulty rotor identified as current. Model validation may be based on a statistical test examining the residual uncorrelatedness (whiteness) via the statistical hypothesis testing problem:

$$\begin{array}{lcllll} H_0 & : & \rho_V[\tau]=0 & \tau=1,2,...,r & \text{Rotor V fault} \\ H_1 & : & \rho_V[\tau]\neq 0 & \text{for some } \tau & \text{Not Rotor V fault} \end{array} \quad (26)$$

in which $\rho_V[\tau]=0(\tau=1,2,...,r)$ designates the residual series normalized autocorrelation at lag τ. Under the null hypothesis the following Q statistic follows a chi-square (χ^2) distribution with r degrees of freedom (Ref. 31):

$$Q = N(N+2)\cdot\sum_{\tau=1}^{r}(N-\tau)^{-1}\cdot\widehat{\rho}[\tau]^2 \sim \chi^2(r) \quad (27)$$

in which N designates the residual signal length (in number of samples),$\widehat{\rho}[\tau]$ the estimated normalized autocorrelation at lag, τ and r the maximum lag. This leads to the

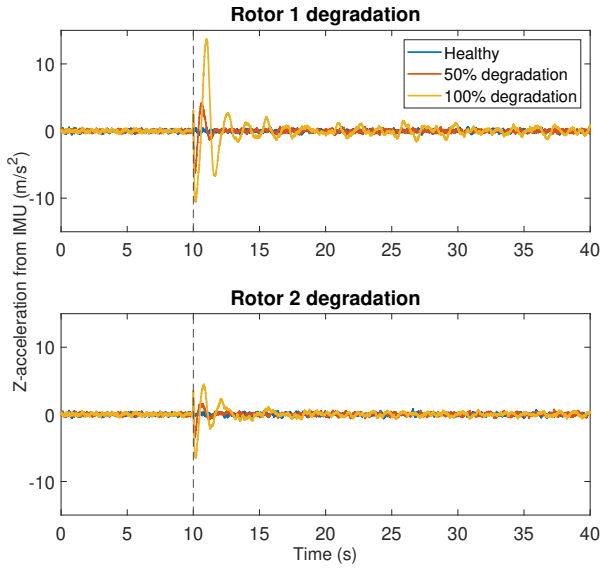

Figure 4: Z-acceleration signals from IMU for different rotor fault states.

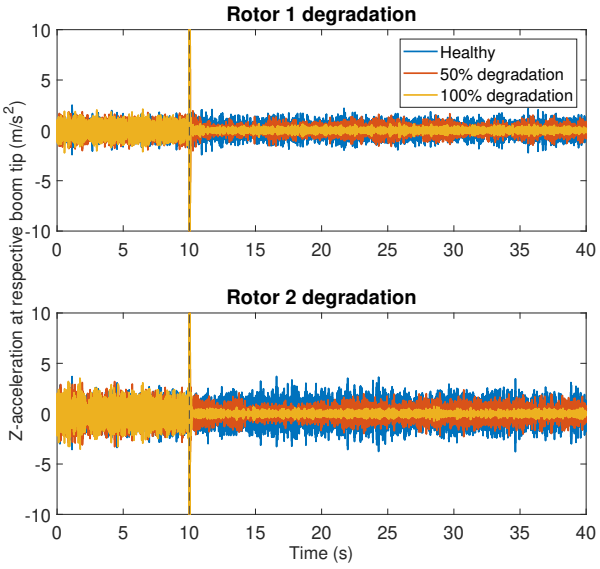

Figure 5: Z-acceleration signals at respective boom tip for different rotor fault states.

following test at the α risk level:

$$\begin{aligned} \chi^2_\rho \leq \chi^2_{1-\alpha}(r) \quad &\Longrightarrow H_0 \text{ accepted (rotor V is faulty)} \\ \text{Else} \quad &\Longrightarrow H_1 \text{ accepted (rotor V is not faulty)} \end{aligned} \tag{28}$$

where $\chi^2_{1-\alpha}(r)$ denotes the χ^2 distribution's $1-\alpha$ critical point.

It should be noticed that inability to identify a particular rotor fault (obviously as not previously modeled) indirectly implies fault detection.

Fault Quantification (Magnitude Estimation) Fault quantification (magnitude estimation) is then based on the interval estimate of k, constructed based on the $\hat{k}$, $\hat{\sigma}^2{}_k$ estimates obtained from the corresponding re-parameterized FP-AR model (of the form Eq.20) of the current valid rotor fault. The interval estimate of k (fault magnitude) at the α risk level is given as:

$$\left[k + t_{\frac{\alpha}{2}}(N-1)\hat{\sigma}_k \qquad k + t_{1-\frac{\alpha}{2}}(N-1)\hat{\sigma}_k\right] \tag{29}$$

where t_α designates the t distribution's (with the indicated degrees of freedom) α critical point (defined as $\mathbb{P}\left[t \leq t_\alpha\right] = \alpha$) and $\hat{\sigma}_k$ is the positive square root of the obtained variance $\hat{\sigma}^2_k$.

RESULTS AND DISCUSSION

Data Generation

Flight simulation for the hexacopter was performed at operating ranges specified in Table 1 with severe turbulence according to the Dryden model. Figures 4 and 5 show time histories of z-acceleration from the aircraft IMU (global sensors/signals) and accelerometers placed at the respective boom tip (local sensors/signals), respectively, for cases of healthy flight, 50% degradation and complete failure of rotors 1 and 2. The local sensor readings, i.e., the z-acceleration at the boom tip is placed at the tip of boom 1 and 2, are used for analyzing rotor 1 and 2 faults, respectively. The global sensor readings, which is the z-acceleration obtained from the aircraft IMU, are also used for fault diagnosis of both types of rotor faults, and compared with the corresponding of the local sensors. For the simulation results presented, rotor failure occurs at $t = 10$ s, is indicated by the vertical dashed line. It should be noted that due to faults, the signals show a sharp transient response before settling down to a controller-compensated steady state. Fault detection takes place in the transient part of the signal, whereas the identification and quantification takes place in the fault compensated steady state since the models are suitable for modeling stationary signals only.

Non-Parametric Analysis of signals

Initially, the non-parametric analysis of the signals is presented in the frequency domain to provide a preliminary idea of the aircraft dynamics under the different rotor states. The Welch-based Power Spectral Density (PSD) for the global and local signals, shown in Figures 4 and 5, revealed two dominant modes, i.e., the important dynamics of the system lie in the range of $[0.02 - 1250]$ Hz. Hence, the signals were filtered through a low-pass filter at 1600 Hz and subsequently downsampled from an origi-

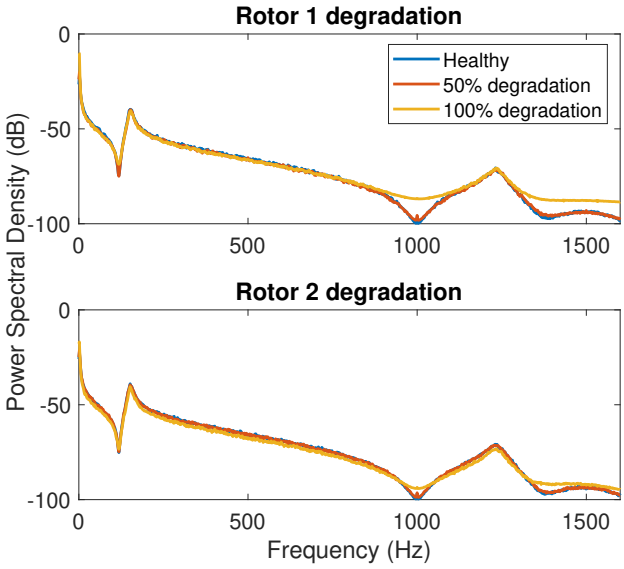

Figure 6: Power spectral density of fault-compensated z-acceleration signals from IMU (global signals) for different rotor fault states.

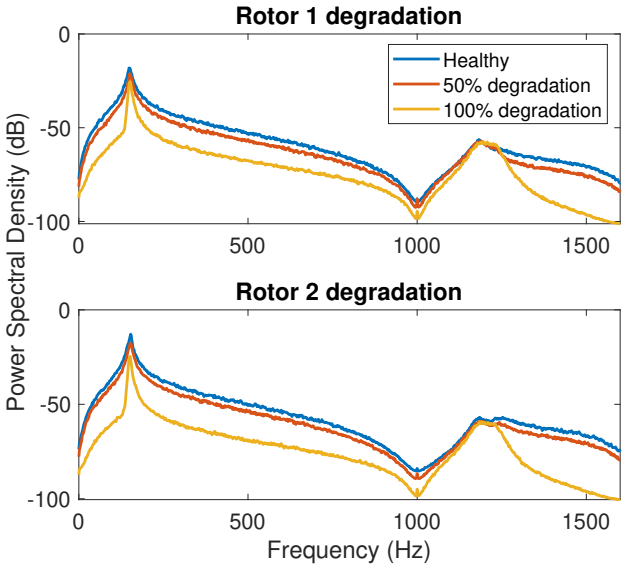

Figure 7: Power spectral density of fault-compensated z-acceleration signals at the respective boom tips (local signals) for different rotor fault states.

nal sampling frequency of $F_s = 10$ kHz to $F_s = 3333$ kHz, such that the frequency range of interest is $[0-1666]$ Hz.

The PSD of the global and local signals, shown in Figures 6 and 7, respectively were obtained by the Welch method for a signal length N of 40 s ($F_s = 3333$ Hz, window size of 2000 samples, nfft of 2000 samples, overlap of 95%; Matlab function *pwelch.m*). The z-acceleration at the boom tip depends predominantly on the out-of plane bending mode dynamics of each boom (states: $\ddot{\eta}_{w_1}$ and $\ddot{\eta}_{w_2}$). Therefore, the first two natural frequencies of boom 1 and 2, can be clearly seen from Fig. 7, and tabulated in Table 2 for booms 1 and 2 for three indicative degradation of the respective rotor placed on them.

FP-AR Model Identification

The FP-AR model identification is based on stationary signals, i.e., their statistical properties remain constant over time. The signals become stationary after approximately 5 s from the fault commencement due to controller compensation and these are used in the modeling stage. Hence, for rotor fault identification and quantification, only steady-state signals should be used. For FP-model estimation for different rotor fault types, data at 0, 20, 40,...,100 % degradation of that rotor at forward velocity of 5 m/s, and 2 kg gross weight was used. First, conventional AR models representing the aircraft dynamics are obtained through standard identification procedures (Refs. 29, 32) based on the signals ($N = 5000$ samples, Matlab function *arx.m*) for the healthy and fault-compensated complete rotor failure states. This is a preliminary step required for providing approximate model orders for the corresponding functionally pooled models representing the aircraft dynamics for the entire range of degradation. Next, the functionally pooled model for the rotor faults is based on either global or local signals of the same length obtained from a total of $K_1 = 6$ simulations, for covering the entire range of the respective rotor degradation. Functional basis order selection starts with the maximum functional search space consisting of 6 Chebyshev Type II polynomial basis functions (see Appendix A). The final functional basis order selection is based on the minimum BIC criterion and the selected model is validated by checking the whiteness (uncorrelatedness) and the normality of the model residuals (Matlab functions *acf.m* and *normplot.m*, respectively) for all the fault magnitudes considered (Refs. 18, 20).

Table 2: Effect of rotor degradation on the respective boom modes.

Boom	Rotor Degradation (%) *(1st mode / 2nd mode* in Hz)		
	0	50	100
1	148 / 1183	151 / 1190	152 / 1196
2	154 / 1183	152 / 1186	150 / 1199

In this section, indicative results for FP model identification of rotor 1 faults with global sensor signals are

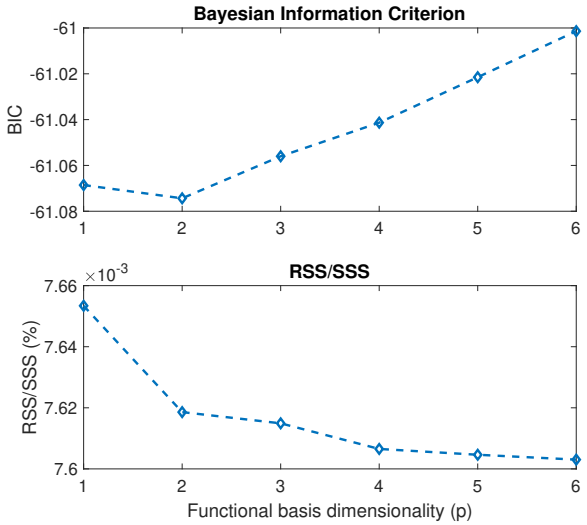

Figure 8: FP-AR Model Structure Selection

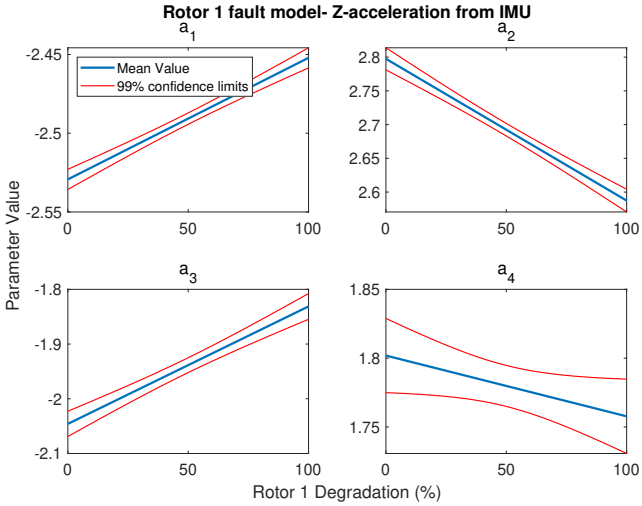

Figure 9: FP-AR Model parameters vs degradation

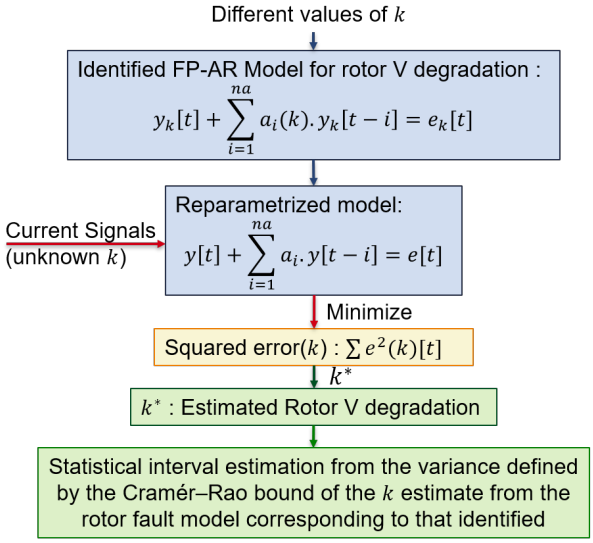

Figure 10: Model residual-based rotor degradation estimation

discussed. First, the model order has been selected as $na = 43$ via the BIC from the z-acceleration signals obtained from the IMU of a healthy aircraft. Next, the functional order was selected as ($p = 2$) based on the minimum BIC criterion (Eq. 18), as depicted in Fig. 8. This implies that the model parameters representing the aircraft vary linearly with the extent of front rotor degradation. This is also reflected in Fig. 9, which shows the first 4 parameters of the FP-AR$(43)_2$ model of rotor 1 faults as a continuous function of the fault magnitude. Also, this model exhibits a very low RSS/SSS value of $7.6 \times 10^{-3}\%$ (Fig. 8) demonstrating accurate identification and excellent dynamics representation of the aircraft z-acceleration signals at modeled rotor 1 faults and severe turbulence.

The FP-AR models for rotor 1 and 2 faults estimated with the global and local signals obtained from the post-failure fault-compensated stationary state are identified in a similar way. The global models are identified with $N = 5000$ samples of the signals. However, the local signals are very sensitive to rotor degradation. Therefore the local models are identified with $N = 1000$ samples as a longer signal is not required for effective model estimation. This also results in improved generalization capability, ensuring that the models can account for the uncertainty in the signals. The summary of all the models employed in this study is provided in Table 3.

Table 3: Model identification summary results.

Fault Type	Signals Used	Model Selected	Samples per Parameter
Rotor 1 Faults	Global	FP-AR$(43)_2$	58
	Local	FP-AR$(16)_2$	31
Rotor 2 Faults	Global	FP-AR$(38)_2$	65
	Local	FP-AR$(12)_2$	41

Model order is denoted in brackets
Functional order is denoted in subscript

Fault detection, identification, and quantification

In the online monitoring phase, the current (unknown) signals are filtered through the baseline models to obtain the corresponding residuals, and the fault detection, identification, and quantification is followed by inspecting the properties of those residuals as shown in Fig. 3. Note that for fault detection and identification it is convenient to use global signal since the same signals can be filtered through both models M_1 and M_2. If we use the local signals for this step, this process needs to run in parallel twice, once with the signals obtained from boom 1 and the other with signals obtained from boom 2. The

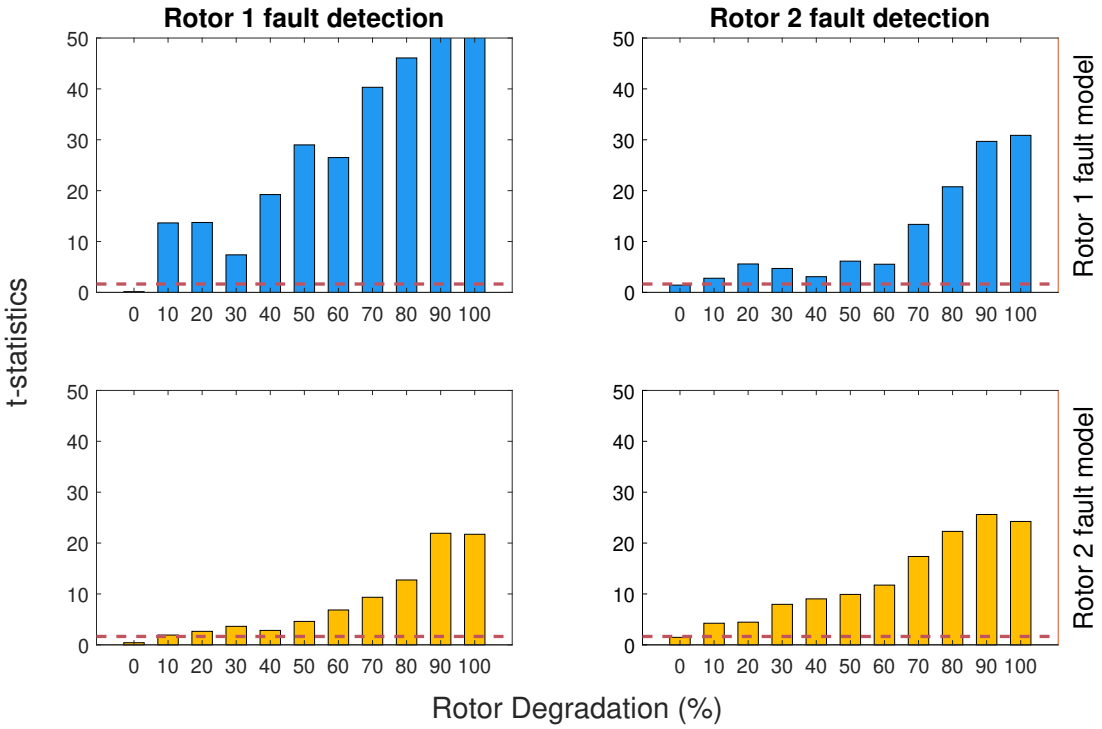

Figure 11: Indicative fault detection results for different rotor faults and various degradation levels. The t-statistics obtained via the rotor 1 and 2 models are shown by blue and yellow bars, respectively. The critical point at the $\alpha = 0.05$ risk level is shown by the red dashed horizontal lines. A fault is detected if the t-statistics exceed the critical point.

complexity may increase with more types or modes of faults considered in later studies. The local signals can be used for better fault quantification, once the fault is identified and it is known that the signals coming from which boom needs to be analyzed. Since the rotor thrust will decline with rotor degradation, it is hypothesized that the local signals can capture the change in dynamics with rotor fault magnitude in a more sensitive fashion. Note that for the fault detection and identification results discussed, the signals used are global signals, unless specified otherwise. The performance of fault quantification has been assessed for both global and local signals.

In this method, the current (unknown) signals are filtered through the different rotor fault type models, reparameterized with all possible values of rotor degradation. The estimation of rotor degradation for different fault types is obtained through minimizing the one-step-ahead prediction error, as illustrated in Fig. 10. Next, the fault diagnosis proceeds in three steps: detection, identification or classification, and quantification, as discussed in the following sections.

Fault Detection Fault detection is achieved in an online, real-time manner through taking a 1 s ($N = 3333$ samples) moving window of the current signal with the window being updated every 0.1 s. Then, the windowed data is used to estimate the rotor degradation values, $\hat{k_{1u}}$ and $\hat{k_{2u}}$ and their corresponding variances from M_1 and M_2, respectively. These are used to construct the corresponding t-statistics given by Eq. 24, and the statistical limit is constructed at $\alpha = 0.05$ to perform the hypothesis testing to determine faults (Eq. 25).

Figure 11 shows indicative fault detection for a single time window, at the instant of fault initiation, for both rotor 1 and 2 and fault magnitude ranging from healthy to complete failure. The t-statistics obtained via model M_1 and M_2 are shown in blue and yellow bars respectively. The critical limit is shown in red dashed horizontal lines. It has been observed that the fault detection is fast, within 2 s of the fault commencement. In this figure, the first and second columns of the subplots presents the fault detection results for the rotor 1 and 2 fault signals, respectively. The top and bottom row are for the rotor 1 and 2 models, respectively being used to filter and analyze the signals. The signals for rotor degradation of 0% yield t-statistics that lie below the critical limit, for both M_1 and M_2, correctly denoting that the aircraft is healthy. For 10% degradation of rotor 1, the test statistics obtained with the rotor 2 fault model lie below the critical limit (as seen in the bottom-left figure), but it is detected via the

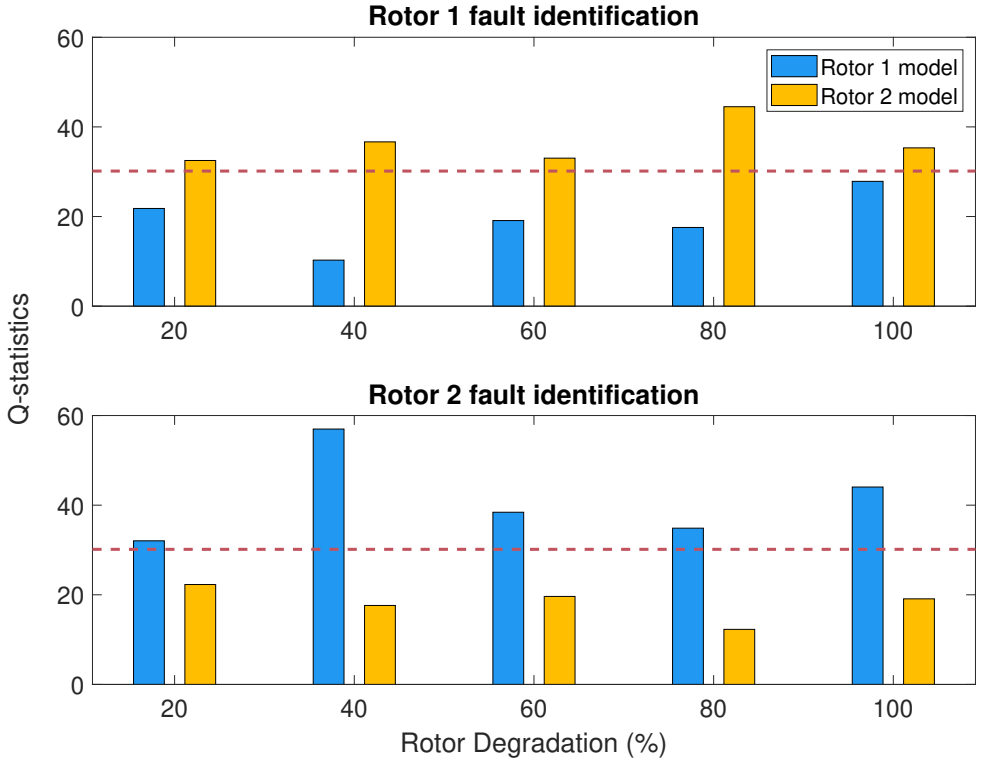

Figure 12: Indicative fault identification results for different rotor faults and degradation levels. The Q-statistic for the hypothesis of the current fault belonging to rotor 1 or 2 is shown in blue and yellow bars, respectively. The critical point at the $\alpha = 0.05$ risk level is shown by the red dashed horizontal lines. A hypothesis is accepted –and the corresponding rotor fault is accepted as true– if its Q-statistic lies below the critical point.

rotor 1 fault model. For all other rotor degradation, the test statistics exceed the statistical limit, thereby detecting a fault.

Fault Identification Once a fault is detected, the identification is performed only after the fault is compensated by the controller because the identified models represent the steady-state dynamics. This is determined by monitoring the signal variance, which is high during the transient response but settles down to a low and constant value when they become stationary again (Refs. 20, 32). After that 5 s of fault-compensated global z-acceleration signal is used for estimating rotor degradation via the two models M_1 and M_2, denoted as $\hat{k_{1u}}$ and $\hat{k_{2u}}$ respectively. The same signal filtered through M_1 re-parameterized by $\hat{k_{1u}}$ and M_2 by $\hat{k_{2u}}$ to generate two sets of residuals. The fault is classified as the one for which the resulting residuals are white or serially uncorrelated.

Indicative rotor fault identification results for "unmodeled" fault magnitude (20, 40, 60, 80 and 100% degradation) are presented in Fig. 12. The hypotheses of the current fault belonging to rotor 1 or 2 using the corresponding FP-AR model are presented in the blue and yellow bars respectively. The autocorrelation function of the two residual sequences with maximum lag $\tau = 20$ has been considered as the test statistics. One of these hypotheses is accepted if the corresponding Q-statistic is lower than the 95% statistical limit shown in the red dashed horizontal line (Eq. 27 and 29). It is observed that for signals corresponding to rotor 1 degradation the rotor 1 fault model (re-parameterized by $\hat{k_{1u}}$) yields white residuals whereas the rotor 2 model (re-parameterized by $\hat{k_{2u}}$) yields correlated residuals shown by the blue bars lying below the critical limit and the yellow bars violating the critical limit, respectively in the top subplot of Fig. 12. Similarly, correct fault identification for rotor 2 faults of varying magnitude has been demonstrated in the bottom subplot.

Fault Quantification (Magnitude Estimation) Next, fault quantification is performed via the identified faulty rotor model, M_V reparameterized with the corresponding degradation estimate, k_{Vu}, where $V = 1$ or 2. It has been observed that with the z-acceleration signal from the aircraft IMU accurate quantification can be achieved with 5 s of steady-state fault-compensated signals. The effec-

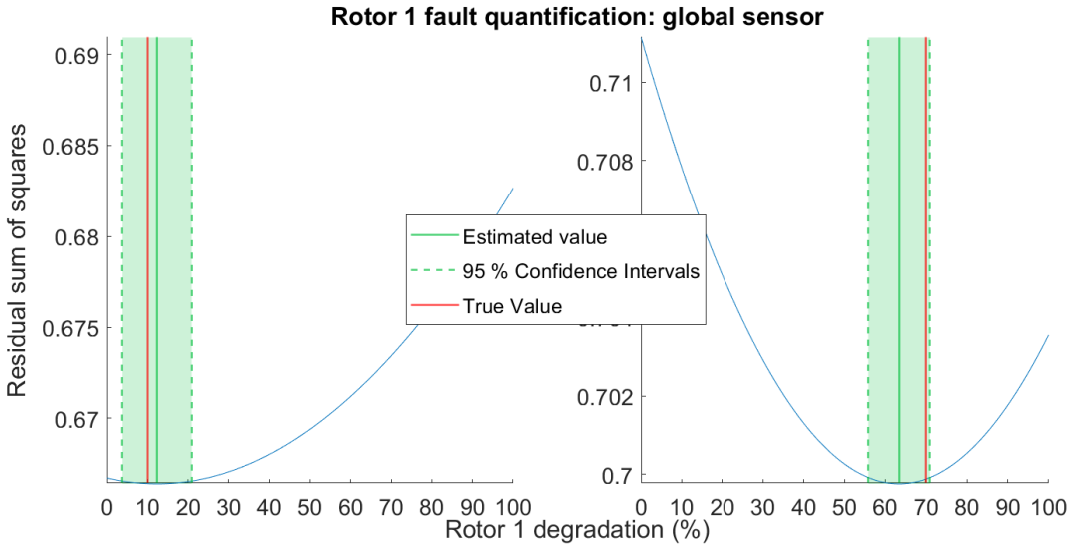

Figure 13: Indicative rotor 1 fault quantification based on global signals (IMU z-acceleration) along with the corresponding 95% confidence intervals. The true value of degradation lies between the 95% confidence intervals, implying correct fault magnitude estimation.

tiveness of the fault diagnosis method is now assessed with a few indicative rotor degradation results. It should be noted that the fault magnitudes in these results do not coincide with those used in the baseline (training) phase. Figure 13 shows indicative fault quantification results of rotor 1 at "unmodeled" degradation levels of 10 and 70 % with the global signal. In this figure, the rotor 1 fault has been estimated with one window of 5 s of the global signal. The estimated value being shown by the green vertical line corresponds to the minimum residual sum of squares or the squared error (shown by the light blue curve) obtained via the global rotor 1 fault model (FP-AR$(43)_2$). The 95% confidence region is shaded in green (Eq. 29), and the true value of the fault magnitude shown by the red vertical line lies in between them, demonstrating correct fault quantification at both indicative fault magnitudes. The width of 95% confidence intervals, in case of fault magnitude estimation with a various time windows of the global signal, ranges from about 16 to 20%.

As discussed before, this step is performed after fault identification, and the local signals, corresponding to the boom on which the faulty rotor is located, can also be used. Figure 14 show the fault quantification of rotor 1 at the same degradation levels as Fig. 13, but with the local signal. When the z-acceleration measured at boom 1 tip is used with the local rotor 1 fault model (FP-AR$(16)_2$), even 1 s of signal window can accurately quantify rotor 1 degradation. Here, the estimated fault magnitude, $\hat{k}$ from for one such time window of the local signal is shown by the blue vertical line. The 95% confidence region is shaded in blue, and the true fault magnitude lies in that region, which is observed to be about 60% narrower than that obtained with the global signal. Therefore, fault quantification with the local signal is faster (lesser signal length), more accurate, and precise.

Similar results have been obtained with rotor 2 faults, and a few indicative cases for it will be discussed in the context of comparing the fault quantification performance of global and local signals.

Comparison between local and global sensors for fault quantification

From Figures 13 and 14, it is evident that the local signals are more sensitive to the rotor 1 fault magnitude. This has also been verified by rotor 2 fault quantification at two indicative fault magnitude of 20% and 80% with the z-acceleration from IMU and the z-acceleration of the boom 2 tip signals. For comparison of the effectiveness of fault quantification by local and global signals 2 s window of both are analysed by their corresponding baseline models, and the results are presented in Fig. 15. It can be clearly seen that local sensors outperform the global sensors in both accuracy and precision of fault quantification for both front and side rotor. Accuracy is defined by the difference between the estimated and the true value of degradation and the precision is defined by the tightness of the statistical confidence interval. The average error of estimation with global signal is 5.55% and the average width of uncertainty interval is 18.44%. These figures improve when local signals are used, with average

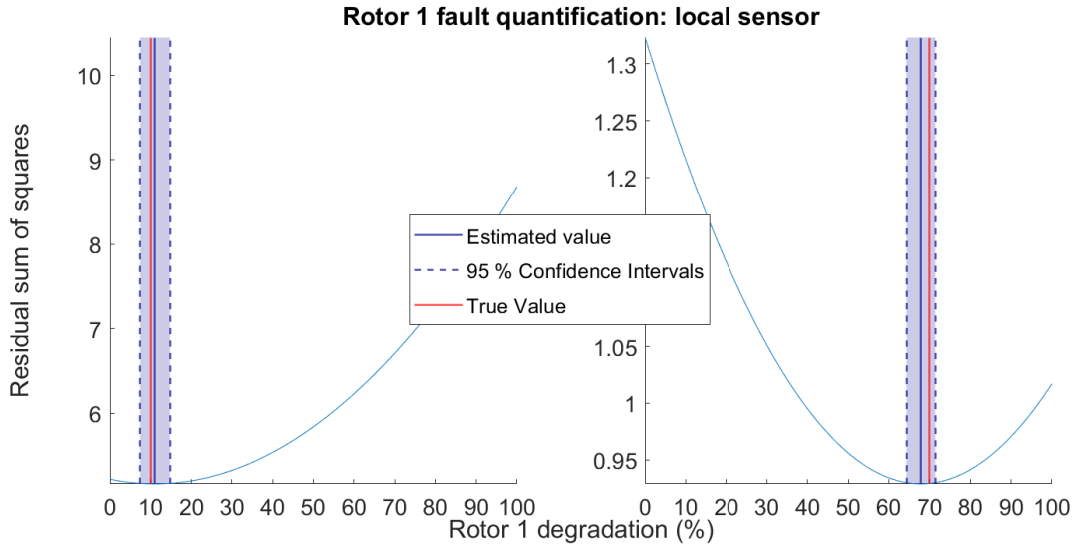

Figure 14: Indicative rotor 1 fault quantification based on local (boom z-acceleration) signals along with the corresponding 95% confidence intervals. The true value of degradation lies between the 95% confidence intervals, implying correct fault magnitude estimation.

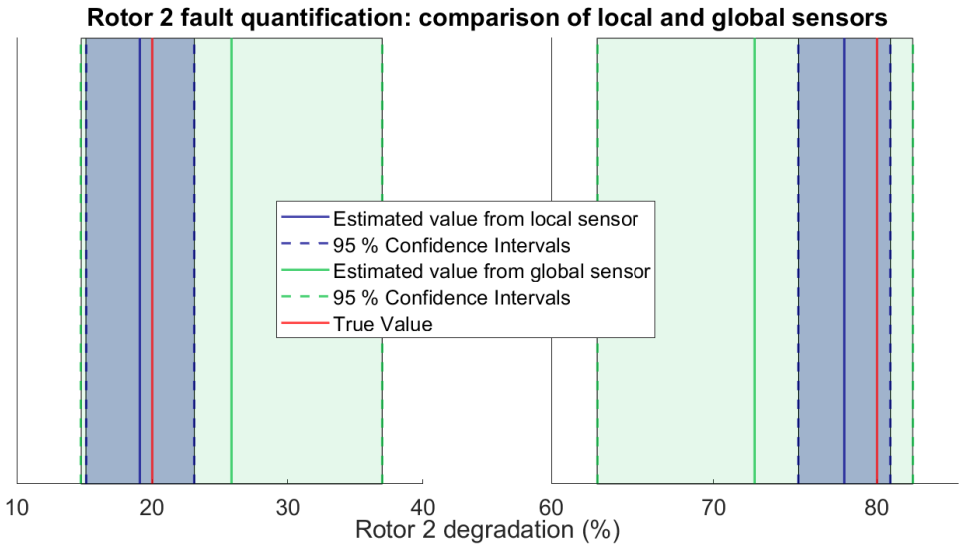

Figure 15: Comparison of rotor 2 fault quantification via global and local signals. Correct fault magnitude estimation has been achieved by both the sensors. Local signals show improved accuracy and narrower confidence intervals than the global signals.

error of 1.55% and the average statistical confidence intervals range of 7.05%. These values are calculated from estimation results from several time windows and fault magnitudes.

CONCLUSIONS

A sensor signals based statistical time series method that is capable of effective fault detection, identification, and magnitude estimation within a unified framework is introduced. The method is based on the FP models and proper statistical decision-making schemes. FP models are capable of accurately representing an aircraft under rotor faults for a continuum of fault magnitudes of a particular rotor fault type. These models for different rotor faults on a multicopter can be identified from available time-series sensor data in the baseline phase. In its inspection phase, there are three distinct steps taking place within a probabilistic framework: step I involves fault detection, step

II involves fault identification, and step III involves precise fault quantification within the identified type of fault. Fault magnitude is continuous, involving an infinite number of potential fault magnitudes ranging from healthy to complete failure. The validity and effectiveness of the method have been assessed via a proof-of-concept application to rotor fault diagnosis on a hexacopter. Front and side rotor degradation of different magnitudes occurring on the aircraft was simulated by reducing the commanded rotor speed. Indicative results for "unmodeled" rotor degradation shows that the method is effective in detecting abrupt faults, identifying the correct faulty rotor, and then determining the fault magnitude precisely while providing estimation uncertainty bounds.

The main conclusions drawn from this study are summarized as follows:

- The study – including the proof-of-concept application – has demonstrated that effective fault detection, fault mode identification, and fault magnitude estimation are possible based on partial models of the aircraft dynamics and a very limited number of sensors (even with a single response signal from the IMU). This is in sharp contrast to methods requiring detailed and "complete" models (such as analytical models) and a multitude of sensors.
- In addition, the study has substantiated that a significant amount of information about the health state of the aircraft is available even in a single response signal (here, body and boom accelerations). Thus, an important message is that it may not be necessary to employ a "high" number of sensors for precise fault diagnosis; instead, a "few" sensors and powerful signal analysis for extracting the embedded information may be much more practical and effective approach.
- Robust rotor fault detection, identification, and quantification for a hexacopter in forward flight have been achieved under severe turbulence based on predetermined statistical confidence levels.
- An important observation is that fault quantification performance is improved via the use of local sensors (boom accelerations) compared to global sensors (body acceleration), as indicated by the accuracy of fault size estimation and tighter uncertainty bounds.
- The method may operate on any type (acceleration, rate gyros, strain gauges) of sensor signals.

AUTHOR CONTACT

Airin Dutta duttaa5@rpi.edu
Robert Niemiec niemir2@rpi.edu
Fotis Kopsaftopolous kopsaf@rpi.edu
Farhan Gandhi fgandhi@rpi.edu

ACKNOWLEDGMENT

This work was supported by the U.S. Air Force Office of Scientific Research (AFOSR) grant "Formal Verification of Stochastic State Awareness for Dynamic Data-Driven Intelligent Aerospace Systems" (FA9550-19-1-0054) and Program Officer Dr. Erik Blasch.

REFERENCES

1. Booz, Allen, and Hamilton, "Urban Air Mobility (UAM) Market Study," Technical report, NASA, November 2018.
2. "Fast-Forwarding to a Future of On-Demand Urban Air Transportation," Technical report, October 2016.
3. McKay, M., Niemiec, R., and Gandhi, F., "Post-Rotor-Failure-Performance of a Feedback Controller for a Hexacopter," American Helicopter Society 74th Annual Forum, Phoenix, AZ, May 2018.
4. Stepanyan, V., Krishnakumar, K., and Bencomo, A., "Identification and Reconfigurable Control of Impaired Multi-Rotor Drones," AIAA Science and Technology Forum and Exposition, January 2016.
5. Frangenberg, M., Stephan, J., and Fichter, W., "Fast Actuator Fault Detection and Reconfiguration for Multicopters," AIAA Guidance, Navigation, and Control Conference, January 2015. DOI: 10.2514/6.2015-1766
6. Sadeghzadeh, I., Chamseddine, A., Zhang, Y., and Theilliol, D., "Control Allocation and Reallocation for a Modified Quadrotor Helicopter against Actuator Faults," *IFAC Proceedings Volumes*, Vol. 45, (20), 8th IFAC Symposium on Fault Detection, Supervision and Safety of Technical Processes, 2012, pp. 247 – 252. DOI: https://doi.org/10.3182/20120829-3-MX-2028.00291
7. Freddi, A., Longhi, S., and Monteriù, A., "Actuator fault detection system for a mini-quadrotor," 2010 IEEE International Symposium on Industrial Electronics, 2010. DOI: 10.1109/ISIE.2010.5637750
8. Nguyen, N. P., Mung, N. X., and Hong, S. K., "Actuator Fault Detection and Fault-Tolerant Control for Hexacopter," *Sensors*, Vol. 19, (21), 2019. DOI: 10.3390/s19214721

9. Heredia, G., and Ollera, A., "Sensor Fault Detection in Small Autonomous Helicopters using Observer/Kalman Filter Identification," IEEE International Conference on Mechatronics, Malaga, Spain, April 2009.

10. Qi, X., Theillol, D., Qi, J., Zhang, Y., and Han, J., "A Literature Review on Fault Diagnosis Methods for Manned and Unmanned Helicopters," International Conference on Unmanned Aircraft Systems, May 2013.

11. Fassois, S., and Kopsaftopoulos, F., *New Trends in Structural Health Monitoring*, Springer, January 2013, Chapter Statistical Time Series Methods for Vibration Based Structural Health Monitoring, pp. 209–264. DOI: 10.1007/978-3-7091-1390-5

12. Kopsaftopoulos, F. P., and Fassois, S. D., "Scalar and Vector Time Series Methods for Vibration Based Damage Diagnosis in a Scale Aircraft Skeleton Structure ," *Journal of Theoretical and Applied Mechanics*, Vol. 49, (4), 2011.

13. Samara, P. A., Fouskitakis, G. N., Sakellariou, J. S., and Fassois, S. D., "A Statistical Method for the Detection of Sensor Abrupt Faults in Aircraft Control Systems," *IEEE Transactions on Control Systems Technology*, Vol. 16, (4), July 2008, pp. 789–798. DOI: 10.1109/TCST.2007.903109

14. Kopsaftopoulos, F. P., and Fassois, S. D., "A vibration model residual-based sequential probability ratio test framework for structural health monitoring," *Structural Health Monitoring*, Vol. 14, (4), 2015, pp. 359–381.

15. Dimogianopoulos, D., Hios, J., and Fassois, S., "Fault Detection and Isolation in Aircraft Systems Using Stochastic Nonlinear Modelling of Flight Data Dependencies," *Mediterranean Conference on Control and Automation*, Vol. 0, 06 2006, pp. 1–6. DOI: 10.1109/MED.2006.328695

16. Dimogianopoulos, D. G., Hios, J. D., and Fassois, S. D., "FDI for Aircraft Systems Using Stochastic Pooled-NARMAX Representations: Design and Assessment," *IEEE Transactions on Control Systems Technology*, Vol. 17, (6), November 2009, pp. 1385–1397.

17. Kopsaftopoulos, F. P., and Fassois, S. D., "Vector-dependent Functionally Pooled ARX Models for the Identification of Systems Under Multiple Operating Conditions," IFAC Proceedings, Vol. 45, 2012. DOI: 10.3182/20120711-3-BE-2027.00261.

18. Kopsaftopoulos, F., Nardari, R., Li, Y.-H., and Chang, F.-K., "A stochastic global identification framework for aerospace structures operating under varying flight states," *Mechanical Systems and Signal Processing*, Vol. 98(1), 2018, pp. 425–447. DOI: 10.1016/j.ymssp.2017.05.001

19. Dutta, A., McKay, M., Kopsaftopoulos, F., and Gandhi, F., "Statistical residual-based time series methods for multicopter fault detection and identification," *Aerospace Science and Technology*, Vol. 112, 2021, pp. 106649. DOI: https://doi.org/10.1016/j.ast.2021.106649

20. Dutta, A., McKay, M., Kopsaftopoulos, F., and Gandhi, F., "Rotor Fault Detection and Identification on a Hexacopter under Varying Flight States Based on Global Stochastic Models," Vertical Flight Society 76th Annual Forum, Online (due to COVID-19), October 2020.

21. Dutta, A., McKay, M., Kopsaftopoulos, F., and Gandhi, F., "Fault Detection and Identification for Multirotor Aircraft by Data-Driven and Statistical Learning Methods," Electric Aircraft Technologies Symposium (EATS), Indianapolis, IN, August 2019.

22. Dutta, A., McKay, M., Kopsaftopoulos, F., and Gandhi, F., "Rotor Fault Detection and Identification for a Hexacopter Based on Control and State Signals via Statistical Learning Methods," Vertical Flight Society 76th Annual Forum, Online (due to COVID-19), October 2020.

23. Kopsaftopoulos, F. P., and Fassois, S. D., "A Functional Model Based Statistical Time Series Method for Vibration Based Damage Detection, Localization, and Magnitude Estimation," *Mechanical Systems and Signal Processing*, Vol. 39, 2013, pp. 143–161. DOI: 10.1016/j.ymssp.2012.08.023

24. Peters, D., and He, C., "A Finite-State Induced Flow Model for Rotors in Hover and Forward Flight," American Helicopter Society 43rd Annual Forum, St. Louis, MO, May 1987.

25. Hakim, T. M. I., and Arifianto, O., "Implementation of Dryden Continuous Turbulence Model into Simulink for LSA-02 Flight Test Simulation," Journal of Physics: Conference Series 1005(2018) 012017, August 2018.

26. Greene, W. H., *Econometric Analysis*, Prentice Hall, fifth edition, 2003.

27. Kopsaftopoulos, F. P., and Fassois, S. D., "Vector-dependent Functionally Pooled ARX Models for

the Identification of Systems Under Multiple Operating Conditions," 16th IFAC Symposium on System Identification The International Federation of Automatic Control, Brussels, Belgium, Vol. 46, 2012.

28. Ljung, L., *System Identification: Theory for the User*, Prentice–Hall, second edition, 1999.

29. Dutta, A., McKay, M., Kopsaftopoulos, F., and Gandhi, F., "Rotor Fault Detection and Identification on a Hexacopter Based on Statistical Time Series Methods," Vertical Flight Society 75th Annual Forum, Philadelphia, PA, May 2019.

30. Kopsaftopoulos, F. P., and Fassois, S. D., "A functional model based statistical time series method forvibration based damage detection, localization, andmagnitude estimation," *Mechanical Systems and Signal Processing*, Vol. 39, 2013, pp. 143–161.

31. Box, G. E. P., Jenkins, G. M., and Reinsel, G. C., *Time Series Analysis: Forecasting & Control*, Prentice Hall: Englewood Cliffs, NJ, third edition, 1994.

32. Dutta, A., McKay, M., Kopsaftopoulos, F., and Gandhi, F., "Statistical Time Series Methods for Multicopter Fault Detection and Identification," Vertical Flight Society International Powered Lift Conference, San Jose, CA, Jan 2020.

APPENDIX

A. Signals

The data used in this study are obtained from simulation rather than experiments and therefore the sensor signals need to be calculated from the available aircraft states.

Generally, Inertial Measurement Units (IMUs) are composed of a 3-axis accelerometer and a 3-axis gyroscope and outputs the body accelerations (x, y, and z acceleration) and the angular rates (roll, pitch, pitch and yaw rates), which can be determined from 12 rigid body states are defined in Eq. 1 as follows:

$$\begin{aligned} \text{Body accelerations} &= \begin{bmatrix} \dot{u} & \dot{v} & \dot{w} \end{bmatrix}^T \\ \text{Angular rates, } \omega &= \begin{bmatrix} p & q & r \end{bmatrix}^T \end{aligned} \tag{30}$$

These signals are referred to as global signals.

The sensors mounted on the different locations on the individual booms, such as strain gauges and accelerometers are referred to as the local signals. These can be computed from the individual booms modal deformation

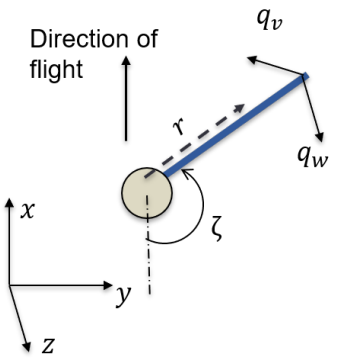

Figure 16: Position of a boom with respect to the hub and its deformations

states and shape functions (Eqs. 5 and 3) using the following expressions:

$$\text{Total deformation, } q = \begin{cases} \sum_{i=1}^{2} \phi_{w_i}(l)\eta_{w_i} & \text{Out-of-plane} \\ \sum_{i=1}^{2} \phi_{v_i}(l)\eta_{v_i} & \text{In-plane} \end{cases}$$

$$\text{Strain, } \varepsilon = \begin{cases} \sum_{i=1}^{2} \phi''_{w_i}(l)\eta_{w_i} \times a/2 & \text{Out-of-plane} \\ \sum_{i=1}^{2} \phi''_{v_i}(l)\eta_{v_i} \times b/2 & \text{In-plane} \end{cases} \tag{31}$$

where, a and b are the width and height of the cross-section of the boom, respectively. l is the distance from the boom root where the sensor has been placed, normalized by the boom length.

Table 4: Boom properties

Parameters	Value
Boom Length (L)	0.2617 m
Material	Aluminium
Cross-section	Hollow square
Outer dimension	0.0156 m
Inner dimension	0.0130 m
Flexural Rigidity	179 Nm^2

The accelerometer readings on each of the boom can be calculated as:

$$\text{Acceleration} = \ddot{r} + \omega \times \dot{r} + \dot{\omega} \times r + \omega \times \omega \times r \tag{32}$$

where,

$$\text{Distance of accelerometer from the hub, } r = \begin{bmatrix} -L\cos\zeta \\ L\sin\zeta \\ -d \end{bmatrix} + \begin{bmatrix} -\sum_{i=1}^{2} \phi_{v_i}(l)\eta_{v_i}\sin\zeta \\ -\sum_{i=1}^{2} \phi_{v_i}(l)\eta_{v_i}\cos\zeta \\ \sum_{i=1}^{2} \phi_{w_i}(l)\ddot{\eta}_{w_i} \end{bmatrix}$$

Here, ζ is the azimuth angle of the boom (See Fig. 16), L is the length of the boom and d is the vertical position of

the boom from the center-of-gravity of the aircraft. The boom properties are given in Table 4.

Note that these derivations are shown for a single time instant, t. Repeating this computations for the entire range of time will generate the time-series sensor data.

B. Basis Functions

The univariate polynomials used in this study in are the shifted Chebyshev polynomials of the second kind (Type II Chebyshev polynomials), which belong to the broader family of Chebyshev orthogonal polynomials. These polynomials obey the following recurrence relation:

$$\begin{aligned} a_{1,n}G_{n+1}(x) &= (a_{2,n}+a_{3,n}x)G_n(x) - a_{4,n}G_{n-1}(x) \\ x &\in [0,1] \subset \mathbb{R} \end{aligned} \tag{33}$$

with $a_{1,n} = a_{4,n} = 1, a_{2,n} = -2, a_{3,n} = 4$, and $G_0(x) = 0, G_1(x) = 1$.

Hence, the first five shifted Chebyshev polynomials of the second kind are:

$$\begin{aligned} P_0 &= 1 \\ P_1 &= -1+2x \\ P_2 &= 1-8x+8x^2 \\ P_3 &= -1+18x-48x^2+32x^3 \\ P_4 &= 1-32x+160x^2-256x^3+128x^4 \end{aligned} \tag{34}$$

In the present framework, where the variable is the rotor degradation (k) and it is scaled as follows:

$$x \in [0,1] \subset \mathbb{R}, \quad x = k/k_{max} \tag{35}$$

C. Cramér-Rao Lower Bound for operating parameter vector, k estimates

For estimation of k from unknown signal, $y_u[t]$:

$$\begin{aligned} y_u[t] &= \sum_{i=1}^{na} a_i(k)\cdot y_u[t-i] + e_u[t,k] \\ \hat{k} &= \arg\min_{k\in\mathbb{R}^1} \sum_{i=1}^{N} e_u^T[t,k]e_u[t,k] \\ \sigma_u^2(\hat{k}) &= \frac{1}{N}\sum_{t=1}^{N} e_u[t,\hat{k}]e_u^T[t,\hat{k}] \end{aligned} \tag{36}$$

Now, $\hat{k}$ is assumed to be asymptotically $(N\to\infty)$ Gaussian distributed with $\hat{k} \sim \mathcal{N}(k,\sigma_k^2)$

The log-likelihood function of $\hat{k}$ based on N samples of unknown signal is given by:

$$\begin{aligned} \ln \mathscr{L}(\hat{k},\sigma_u^2(\hat{k})) = &-\frac{N}{2}ln(2\pi) - \frac{N}{2}ln(\sigma_u^2) \\ &-\frac{1}{2}\sum_{t=1}^{N}\frac{e_u^T(\hat{k}),t)e_u(\hat{k}),t)}{\sigma_u^2(\hat{k})} \end{aligned} \tag{37}$$

The Cramér-Rao Lower bound for σ_k^2 is given by:

$$\begin{aligned} \sigma_{CRLB}^2 &= \left[\mathbf{E}\Big[\Big(\frac{\delta \ln \mathscr{L}(k,\sigma_u^2)}{\delta k}\Big)\Big(\frac{\delta \ln \mathscr{L}(k,\sigma_u^2)}{\delta k}\Big)^T\Big]\right]^{-1} \\ &= \sigma_u^2(k)\left[\sum_{t=1}^{N}\varepsilon(k,t)\varepsilon(k,t)^T\right]^{-1} \end{aligned} \tag{38}$$

where,

$$\varepsilon(k,t) = \frac{\delta e_u^T(k,t)}{\delta k}$$

which can be simplified from Eq. 12 as follows:

$$\begin{aligned} \varepsilon(k,t) &= \frac{\delta\Big(y_u[t] - \big[\varphi_k^T[t]\otimes \mathbf{G}^T(k)\big]\cdot\theta\Big)^T}{\delta k} \\ &= 0 - \theta^T\cdot\varphi_u[t]\otimes\frac{\delta \mathbf{G}(k)}{\delta k} \end{aligned} \tag{39}$$

Finally, the Cramér-Rao Lower bound for the estimated value of k, $\hat{k}$ can be written as:

$$\begin{aligned} \sigma_{CRLB}^2(\hat{k}) &= \sigma_u^2(\hat{k})\left[\sum_{t=1}^{N}\varepsilon(k,t)|_{k=\hat{k}}\varepsilon(k,t)|_{k=\hat{k}}^T\right]^{-1} \\ &= \sigma_u^2(\hat{k})\left[\sum_{t=1}^{N}\big[\theta^T\cdot\varphi_u[t]\otimes\frac{\delta\mathbf{G}(k)}{\delta k}|_{\hat{k}}\big]\big[\theta^T\cdot\varphi_u[t]\otimes\frac{\delta\mathbf{G}(k)}{\delta k}|_{\hat{k}}\big]^T\right]^{-1} \end{aligned} \tag{40}$$